SN Computer Science (2024) 5:72
https://doi.org/10.1007/s42979-023-02395-8

ORIGINAL RESEARCH

Skin Diseases Detection Using LBP and WLD: An Ensembling Approach

Arnab Banerjee[1,2] · Somenath Sarkar[3] · Mita Nasipuri[1] · Nibaran Das[1]

Received: 9 June 2022 / Accepted: 6 October 2023

Abstract

In all developing and developed countries globally, skin diseases are becoming a prevalent health problem for humans of all age groups. Skin diseases create anxiety, affect mental health, worsen working life, and sometimes cause social isolation. Detecting skin diseases in the early stage is very important because early treatment can be helpful in such cases. There are very few dermatologists in rural and semi-urban areas in a country like India. To overcome the problem, a machine learning technique has been developed to detect three prevalent skin diseases—Leprosy, Tinea versicolor, and Vitiligo from the images of the skin lesions. The proposed approach extracts the texture from the images of the skin regions affected by such diseases using Weber's local descriptor and Local binary pattern. Then the representations are ensembled to prepare the feature vector. This ensemble technique achieved 91.38% accuracy using a multilevel support vector machine, using the features extracted from different regions of the skin lesions area utilising the centre of gravity based rotation invariant Weber local descriptor and Local binary pattern. Some popular deep learning networks such as MobileNet, ResNet152, GoogLeNet, DenseNet121, and ResNet101 were used to compare the performance of the proposed approach with the deep learning models. ResNet101 achieved 89% accuracy, i.e. best among all the deep learning models used in this study. The proposed ensemble technique outperformed the top performing deep learning model by 2.38%. This technique will be helpful for the early screening of these skin diseases.

Keywords Pattern recognition · Leprosy · Tinea versicolor · Vitiligo · STM · WLD · WLDRI · LBP · Multi-SVM

Somenath Sarkar, Mita Nasipuri, and Nibaran Das have contributed equally to this work.

This article is part of the topical collection "Advances in Applied Image Processing and Pattern Recognition" guest edited by K C Santosh.

✉ Arnab Banerjee
researchwork.arnab@gmail.com

Somenath Sarkar
dr.somenathsarkar@gmail.com

Mita Nasipuri
mita.nasipuri@jadavpuruniversity.ac.in

Nibaran Das
nibaran.das@jadavpuruniversity.ac.in

[1] Department of Computer Science and Engineering, Jadavpur University, Jadavpur, Kolkata, West Bengal 700032, India

[2] Department of Computer Science and Engineering (Artificial Intelligence and Machine Learning), Dr. B. C. Roy Engineering College, Jemua Road, Fuljhore, Durgapur, West Bengal 713206, India

[3] Department of Dermatology, Venereology and Leprosy, Calcutta School of Tropical Medicine, Kolkata, West Bengal 700073, India

Introduction

Skin diseases have become a big concern for people living in smart cities and industrial areas worldwide. People with skin diseases have a feeling of being cursed and try to stay away from the community. Skin diseases have a very negative impact on an individual's personal, social, and working lives and their family members' lives. The affected people suffer from depression, stress, anxiety, and low self-confidence, which may culminate into a suicidal tendency. In many cases, it has been observed that early detection of diseases may be helpful for doctors to cure a patient comprehensively. In a highly populated country like India, very few dermatologists are available in rural and semi-urban areas. So, keeping all these in mind, an automatic, non-invasive technique to detect skin diseases is essential. Several research works have been done to automatically identify different skin diseases from the images of skin lesions using different pattern recognition and computer vision-based approaches. Preparing a standard automatic or semiautomatic non-invasive technique for identifying different skin diseases

Published online: 07 December 2023

is challenging for several reasons. Very high similarity has been observed in the lesion colors and texture of the areas affected by these skin diseases. In addition, there are significant variations in the lesion colors, texture, and shape of the affected areas from person to person suffering from the same disease. Another problem is the non-availability of a standard database of images of skin lesions for different skin diseases. Some attempts by the researchers to identify diseases from the images of the affected skin area using texture features were reported in [1–4]. Artificial Neural Networks (ANN) and Deep Learning based approaches were used for this purpose in [5–11]. In some of these approaches, patient inputs were taken [5–7, 12] with the skin lesion images for diagnosing the disease. The only disadvantage is that these methods require the strong involvement of some dermatologists to acquire the patient inputs properly during the treatment. In this study, an ensemble of two popular texture extraction techniques, namely, Local Binary Pattern (LBP) and Weber Local Descriptor (WLD) is proposed to enhance the performance of the previous approach [2, 3]. Local binary patterns were used to compute the features from the skin lesion images in [2]. In [3] the skin lesion images were divided into four regions utilising the centre of gravity, and from each of the four images, the rotation invariant WLD features were extracted and then combined. SVM classifier was used in both [2, 3]. This study considered the images of three common skin diseases, namely, Leprosy, Vitiligo, and Tinea versicolor. In addition, the normal skin images were considered in the data set for the experiment. The grid searching technique was applied for the optimal parameter selection of Multi-SVM and used to classify skin diseases. In this work, the proposed method was compared with the Gray-Level Co-Occurrence Matrix (GLCM), Local Binary Pattern (LBP), Discrete Cosine Transform (DCT), Discrete Fourier Transform (DFT), and WLD-based methods for the better establishment of the proposed approach. In addition, the results of the proposed method were compared with some popular deep neural networks such as GoogLeNet, ResNet152, MobileNet, DenseNet121, and ResNet101. This study is organized as follows: Some popular recent works on skin disease identification are presented in Sect. 2. In Sect. 3, the proposed approach, experiment protocols, and results are presented. Finally, the conclusion of this study is given in Sect. 4.

Related Articles

The existing automatic skin disease identification techniques mainly focused on Psoriasis [13], Ringworm [14] and erythemato-squamous [15]. In 2009, Kabari et. al. [5] designed and trained an Artificial Neural Network for skin disease detection in a specific tropical area such as Nigeria. Different patient information and causative organisms were used in the study. In 2011, GLCM was used to detect skin diseases using the extracted feature by Parekh et. al. [1]. They used images of three disease classes from the DERMNET image collection called Atopic Dermatitis, Eczema, and Urticaria. An automatic diagnostic system for six dermatological diseases (Acne, Eczema, Psoriasis, Tinea Corporis, Scabies and Vitiligo) using color skin images and different patient information such as diseased body portion, elevation and the number of occurrences (in months) etc., has been proposed by Shamsul et. al. [12]. It is not a fully automatic method for diagnosing skin diseases, because a dermatologist is always involved here. Another dermatological diagnostic system was introduced in 2012, by Abdul-Rahman et. al. [6], which was based on two feature selection methods—Correlation Feature Selection (CFS), Fast Correlation-based Filter (FCBF) and BPNN (Back Propagation Based Neural Network). This method was tested on six skin diseases—Psoriasis, Seborrheic dermatitis, Lichen Planus, Pityriasis rosea, Cronic dermatitis and Pityriasis Rubra Pilaris. It requires several histopathology inputs from the patient to work on. In 2013, a non-invasive automatic skin disease detection technique using Local Binary Pattern (LBP) was proposed by Nibaran et. al. [2]. A data set with three skin diseases—Leprosy: Tinea versicolor, and Vitiligo, was used for the experiment. Normal skin images were also considered to establish the differences between normal and diseased skin. Another development was introduced by Anabik et. al. [3] in 2013, for detecting Leprosy, Tinea versicolor, and Vitiligo skin diseases using rotation invariant Weber local descriptor. In 2014, another method for detecting skin diseases from skin image samples using ANN was proposed by Yasir et. al. [7]. Different patient inputs like gender, age, liquid type and color, elevation and feeling, were taken for the identification of the diseases. Like [12], this method also requires the involvement of a dermatologist. In 2017, a combination of deep learning and machine learning was employed by Codell et. al. [8] to recognize melanoma from dermoscopy images. An ultra-imaging technique based on photoacoustic dermoscopy was presented by Schwar et. al. [16] in 2017. They used excitation energy and penetration depth measures for skin image analysis. In 2017, Chao et. al. [17] reviewed different techniques that used smartphone applications for Melanoma detection and skin monitoring. They also compared the performance of several apps in terms of performance and image processing techniques used. In 2017, another deep learning-based melanoma detection was proposed by Thao et. al. [9]. They have addressed two problems, segmentation of skin tumours from the skin and classification of skin tumours. Rotation invariant WLD kernel was employed in a deep neural network by Arnab et. al. [18] in 2017. In skin diseases identification, the method achieved 5.74% better accuracy compared to rotation invariant WLD.

In 2018, a non-invasive technique using GLCM for detecting three skin diseases, Herpes, Dermatitis, and Psoriasis, was proposed by Wei et. al. [4]. Deep learning-based classification of skin lesions was proposed by Esteva et. al. [10] in 2017. This method only considered image pixels and corresponding disease labels as input. In 2018, a deep learning-based Melanoma detection technique was proposed Li et. al. [11]. They used two fully convolutional residual networks (FCRN) for lesion segmentation and classification.

Proposed Approach

The proposed study is described in four phases: (1) Preparation of data set of skin lesion images for Leprosy, Vitiligo, Tinea versicolor, and normal skin images. (2) Preprocessing of the images. (3) Feature extraction from the images using the ensemble of LBP and WLD. and (4) Classification of the skin images based on extracted features using Multi-SVM with optimized parameters. The entire process is presented in Fig. 1.

Data Set Preparation

Collecting skin lesion images affected by Leprosy, Tinea Versicolor, and Vitiligo from the patients and preparing a standard data set is the challenging part of this work. It is difficult to get access to these patients and obtain their consent to capture the skin lesion image. In this work, the images of skin lesions from 141 patients were taken. The images were collected from the outdoor patients of the School of Tropical Medicine (STM), Kolkata, for over one year. In this 1-year duration, the images of Leprosy, Vitiligo, and Tinea versicolor affected skin regions were taken from different patients. In case the patient had multiple skin lesions, multiple images from the patient were taken. In addition, the normal skin images were collected to differentiate between normal and diseased skin. All the blurred images were removed from the collection, and only the good images were considered for the experiment. A total of 876 images were considered; out of that, 262 were Leprosy affected skin regions, 210 were vitiligo affected skin regions, 242 were Tinea versicolor affected skin regions, and 162 were normal skin images. The images were taken from the whole skin area affected by skin disease, and then the most prominent affected area was cropped. The data set was partitioned into the training and testing data set in 4:1 proportion. The data collection process was under the supervision of the Computer Science and Engineering department at the Centre for Microprocessor Application for Training, Education, and Research (CMATER), and hence the prepared data set is named JUCMATER: Skindb.v1.

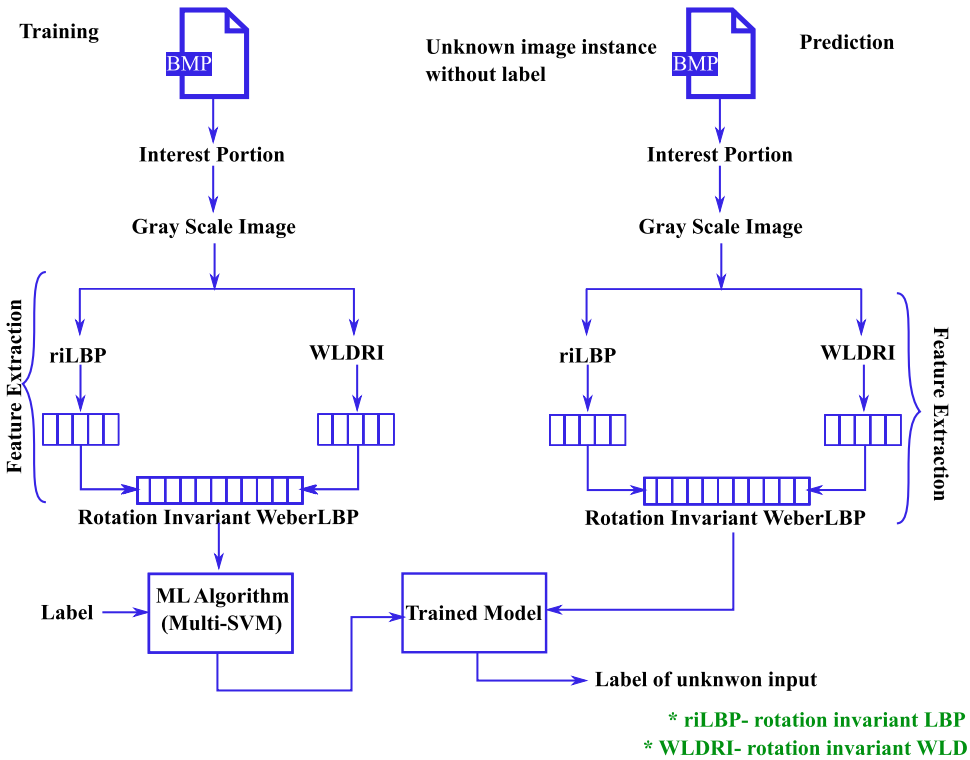

Fig. 1 Overall framework of the proposed approach

Pre-processing

The data set images were cropped and resized to 144×144 to get an equal proportion for the skin lesion. The color images were converted into gray scale images to make the computation easier and less time-consuming. The gray scale images were used as input in the next phase. The BMP file format was used for the images present in the proposed data set.

Feature Extraction

Gray-Level Co-occurrence Matrix (GLCM)

The texture pattern is one of the important features of distinguishing different objects. GrayLevel Co-occurrence Matrix is extensively used as a texture descriptor of an image. The basic idea of Gray-Level Co-occurrence Matrix is calculating the probability of how often a pixel with an intensity value, say x has a specific spatial relationship with another pixel with an intensity value, say y. Basically, the (x,y) entry in Gray Level Co-occurrence matrix contains the spatial relationship probability between x and y at some distance d in the direction θ. The total number of gray levels determines the size of the Gray-Level Co-occurrence matrix. The scaling technique can be used to reduce the number of gray levels in the image. In [19] and [20], different statistical features were computed from the normalized symmetrical images. In the case of directional GLCM, separate co-occurrence matrices are formed for four directions—vertical ($\theta = 90^0$), horizontal ($\theta = 0^0$), left diagonal ($\theta = 135^0$) and right diagonal ($\theta = 45^0$). Now from each co-occurrence matrix, sixteen statistical measures called Energy, Entropy, Inertia, Inverse Difference Moment, Sum Average, Sum of Square Variance, Sum Entropy, Difference Average, Difference Variance, Difference Entropy, Contrast, Correlation, Information Measure of Correlation 1, Information Measure of Correlation 2, Cluster Prominence, Cluster Shade were computed. These measures were used to represent the skin lesion texture.

Discrete Cosine Transform (DCT)

The Discrete Cosine Transform (DCT) separates the image into spectral sub-bands with respect to the image's visual quality. It is a powerful tool for extracting the features from skin lesion images. At first, the DCT was applied to the total skin lesion image, and then some of the co-coefficients were used for making the feature vector. For a $M \times N$ dimensional image, the DCT is calculated as

$$F(a,b) = \frac{1}{\sqrt{MN}}\alpha(a)\alpha(b)\sum_{x=0}^{M-1}\sum_{y=0}^{N-1}Q \\ and\ Q = f(x,y) \times cos\left(\frac{(2x+1)u\pi}{2M}\right) \times \left(\frac{(2y+1)v\pi}{2N}\right) \quad (1)$$

where $a = 0, 1, ... M$ and $b = 0, 1, ... N$ and $\alpha(J)$ is defined by

$$\alpha(J) = \begin{cases} \frac{1}{\sqrt{2}}, & J = 0 \\ 1, & otherwise \end{cases}$$

Discrete Fourier Transform (DFT)

DFT is an important image processing tool to separate the spatial domain image into sine and cosine components. In [21] and [22], the application of DFT was presented as a feature extraction tool. Like DCT, DFT was also applied to the total skin lesion image, and then some of the co-coefficients were used to make the feature vector. The coefficients with global identification capability were taken only. These coefficients encode the compact and orientation independent low-frequency features. For a $M \times N$ dimensional image, DFT was calculated as

$$F(a,b) =) \sum_{x=0}^{M-1}\sum_{y=0}^{N-1} I(x,y) \times e^{-j\frac{2\pi mx}{M}} e^{-j\frac{2\pi ny}{N}} \quad (2)$$

where $j = \sqrt{-1}$

Local Binary Pattern (LBP)

Local binary pattern is a descriptor which uses binary derivatives of a pixel to describe the surrounding relationship of that pixel. It generates a bit-code from the binary derivatives of a pixel. Here we represent the bit-code generation principles by LBP using 3×3 neighborhood pixels. If the neighborhood pixels have greater or equal intensity than the center pixel then 1 will be coded and in the other case, 0 will be coded. An 8-bit binary code was generated, and then depending on the weights, a decimal value will be generated. The process is illustrated in Fig. 2.

While calculating LBP code, the edges with less information are ignored, thus avoiding false information. Although LBP descriptor is explained with only eight pixels in 3×3 neighborhood, it can also be computed with a different

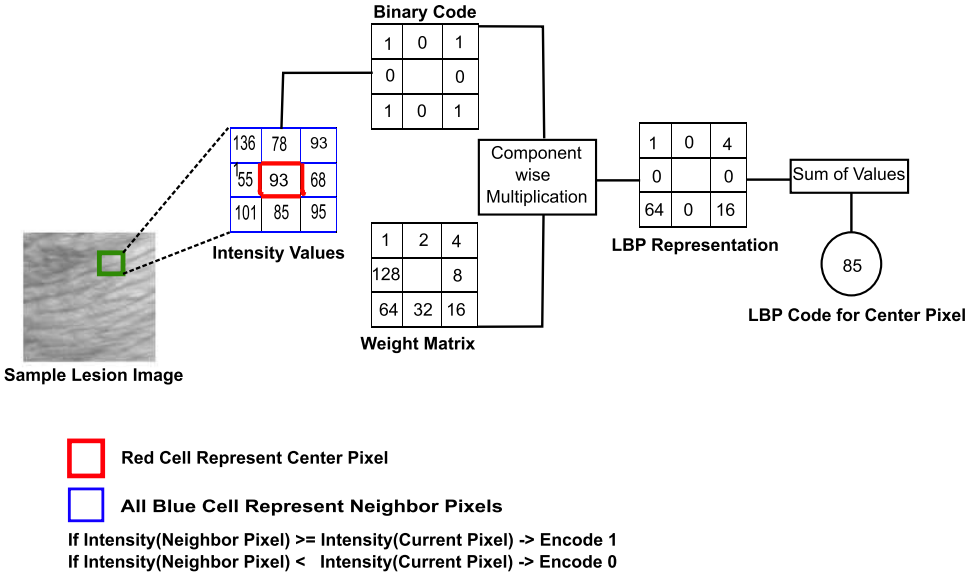

Fig. 2 Working principle of LBP using 3 × 3 neighborhood

radius and a different number of neighboring pixels. In Eq. 3, this concept is presented. Mathematically the traditional LBP can be expressed by Eq. 3:

$$[x_p, y_p] = \left[x_c + Rcos\left(\frac{2\pi p}{P}\right), y_c + Rsin\left(\frac{2\pi p}{P}\right)\right] \tag{3}$$

$$LBP_{P,R} = \sum_{p=0}^{P-1} sign(g_p - g_c.2^p) \tag{4}$$

where P is the number of perimeter pixels and R is the radius of the neighborhood. Here g_p represent the intensities of the surrounding pixels and g_c represent the intensities of the center pixel. The sign(x) function is represented by

$$sign(x) = \begin{cases} 1, & x \geq 0 \\ 0, & otherwise \end{cases}$$

. The rotation invariant LBP can be formed using rotating the bit-code P-1 times and then choosing the minimum decimal equivalent value. The rotation invariant LBP can be represented using $LBP^{ri}_{P,R}$. Mathematically $LBP^{ri}_{P,R}$ can be defined by Eq. 5:

$$LBP^{ri}_{P,R} = minROR(LBP_{P,R}, i) \tag{5}$$

Among all the $LBP^{ri}_{P,R}$ patterns, some of the patterns carry the fundamental properties of the image called the uniform patterns. The uniform LBP patterns can be detected depending on the number of transitions from 0 to 1 or vice versa. If the number of such transitions is less than or equal to 2, then the pattern is called a uniform pattern; otherwise, the pattern is called the non-uniform pattern. Equation 6 formally depicts the relationship:

$$LBP^{riu2}_{P,R} = \begin{cases} \sum_{p=0}^{P-1} sign(g_p - g_c), & if U(LBP_{P,R}) \leq 2 \\ P+1, & otherwise \end{cases} \tag{6}$$

Here, $U(LBP_{P,R})$ can be computed as

$$U(LBP_{P,R}) = |s(g_{p-1} - g_c) - s(g_0 - g_c| + \sum_{p=1}^{P-1} |s(g_p - g_c) - s(g_{p-1} - g_c)| \tag{7}$$

LBP has been extensively applied in different pattern recognition and computer vision tasks like [23–33]. The rotation invariant uniform local binary pattern was applied on the JUCMATER: Skindb.v1 data set. From Fig. 3, the LBP histogram of different skin lesion images can be easily distinguished. As there is a certain variance in different LBP histograms, LBP was used in the proposed approach to classify skin diseases.

Weber Local Descriptor (WLD)

Weber's Law, proposed by Ernest Weber, establishes a constant relationship between incremental threshold and background intensity. Formally, the Weber's law can be expressed by $\frac{\Delta I}{I} = K$, where ΔI is the incremental threshold and I is the initial stimulus intensity. The $\frac{\Delta I}{I}$ is called Weber fraction. WLD is the combination of two components, differential

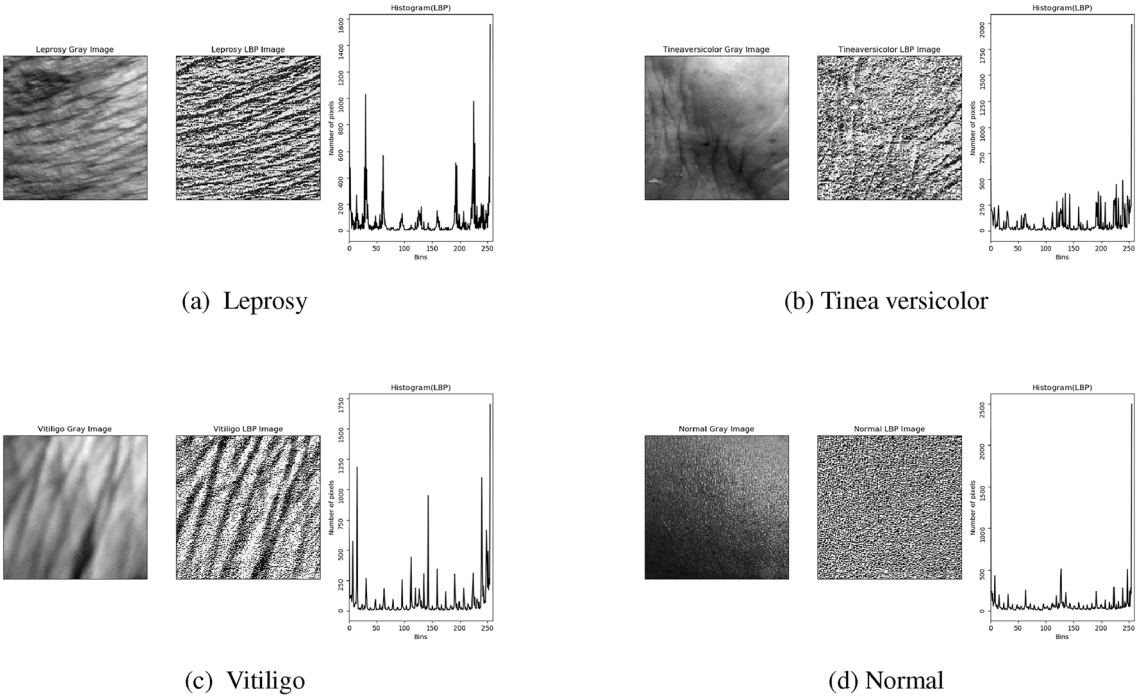

(a) Leprosy (b) Tinea versicolor

(c) Vitiligo (d) Normal

Fig. 3 LBP image and histogram of a sample image from every class

excitation and orientation. The WLD can encode the micro variations between the pixels.

- Differential Excitation: Using differential excitation the micro variations between the intensity values of neighboring pixels can be encoded. Formally, it can be expressed as

$$\Delta I = \sum_{i=0}^{p-1} \Delta I(x_i) = \sum_{i=0}^{p-1} I(x_i) - I(x_c), \tag{8}$$

where ith neighbors of x_c is represented by $x_i (i = 0, 1, ...p-1)$ and p represents total number of neighbors in a region. $I(x_i)$ represent the intensity of the neighboring pixels, and $I(x_c)$ represent the intensity of current pixel. It can be expressed as

$$\xi(x_c) = arctan\left(\frac{\Delta I}{I}\right) = arctan\left(\sum_{i=0}^{p-1}\left(\frac{I(x_i) - I(x_c)}{I(x_i)}\right)\right). \tag{9}$$

If $\xi(x_c)$ is positive, then center pixel is darker with respect to the neighbor pixels, and if $\xi(x_c)$ is negative, then current pixel is lighter with respect to the neighbor pixels.

- Orientation: It determines the directional property of the pixels. It can be computed as

$$\theta(x_c) = arctan\left(\frac{dI_h}{dI_v}\right), \tag{10}$$

where $dI_h = I(x_7) - I(x_3)$, and $dI_v = I(x_5) - I(x_1)$ is calculated from the two filters as in Fig. 2. The mapping of $f : \theta \rightarrow \theta'$ can be expressed as, $\theta' = arctan2(dI_h, dI_v) + \pi$, and

$$f(x) = \begin{cases} \theta, & dI_h > 0 \quad and \quad dI_v > 0 \\ \pi - \theta, & dI_h > 0 \quad and \quad dI_v < 0 \\ \theta - \pi, & dI_h < 0 \quad and \quad dI_v < 0 \\ -\theta, & dI_h < 0 \quad and \quad dI_v > 0, \end{cases} \tag{11}$$

where θ varies from –90° to +90°. The quantization is done using

$$\phi_t = f_q(\theta') = \frac{2t}{T}\pi, where\ t = mod\left(\left\lfloor \frac{\theta'}{\frac{2\pi}{T}} + \frac{1}{2} \right\rfloor, T\right). \tag{12}$$

The working principle of WLD in a 3×3 neighborhood is presented in Fig. 4. A sample 3×3 neighborhood is taken to understand the overall process. The red cell represents the intensity of the center pixel. The ΔI and I filter is applied on the 3×3 neighborhood and differential excitation was calculated using Eq. 9. In the same way, the orientation filters were applied on the 3×3

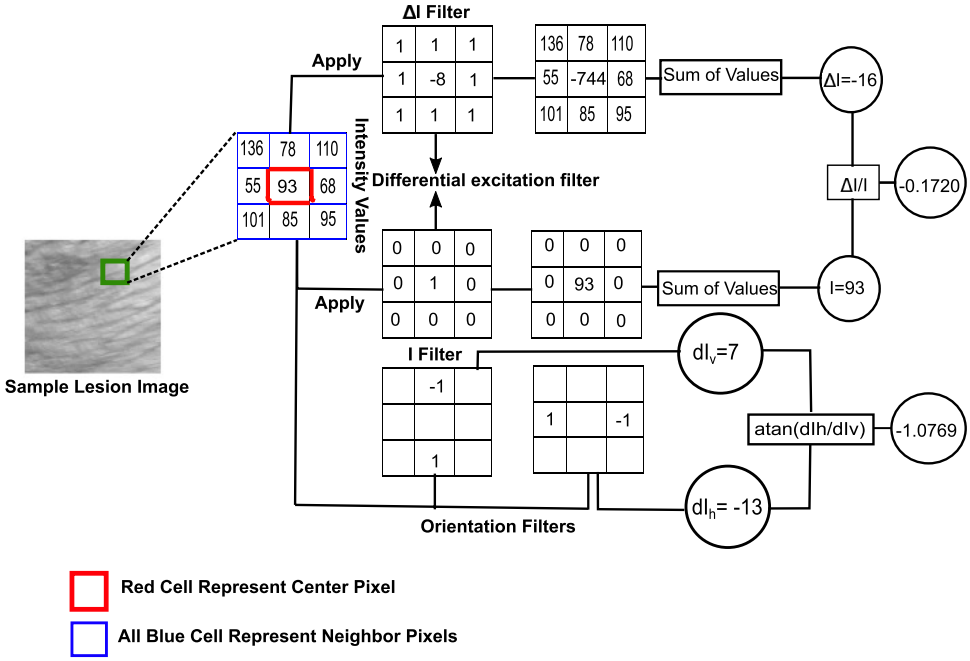

Fig. 4 Illustration how WLD works using 3 × 3 neighborhood

neighborhood and using Eq. 10 the orientation was calculated. Again, rotation invariant WLD can be formed by calculating the orientation component in all eight directions and taking its minimum value. The differential excitation component is inherently rotation invariant because the difference of all neighboring pixels with the center pixel is computed. Formally the rotation invariant WLD (WLDRI) can be expressed by

$$\theta_i = arctan\left(\frac{I(x_{(}(\frac{p}{2}) - i) mod\, p) - I(x_i)}{I(x_{(}(\frac{3p}{4}) - i) mod\, p) - I(x_{(}(\frac{p}{4}) - i) mod\, p)}\right), \text{ and}$$
$$\theta(x_c) = min_{i=0}^{p-1}(\theta_i) \quad (13)$$

- WLD Histogram: The WLD Histogram is constructed separately for the above two components: differential excitation and orientation. Both differential excitation

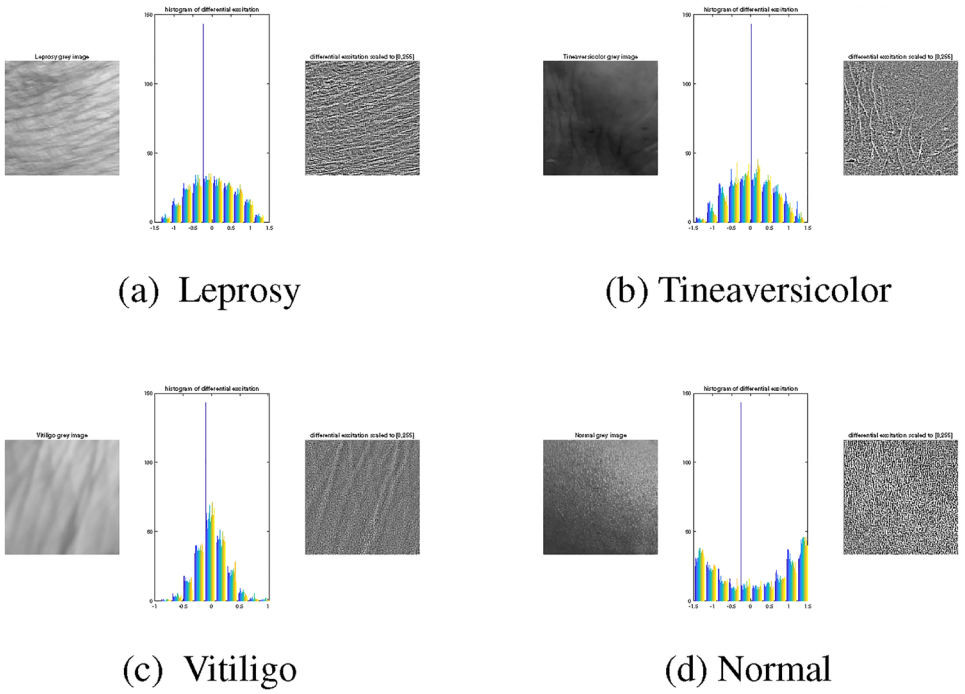

Fig. 5 Histogram and scaled map of differential excitation

and orientation can take the values in the range of $\frac{-\pi}{2}$ to $\frac{\pi}{2}$. The differential excitation values are quantized into T equal width bins, and orientation values are quantized into M equal width bins. The 2D histogram $h_{T,M}$ is formed using the differential excitation and orientation. When the pixels have the same differential excitation and orientation, then the pixels will be put into the same bin. The 2D histogram is converted into the 1D histogram, and the feature vector is formed. In the proposed technique, the parameters T and M carry the values 6 and 8. So, the size of the feature vector becomes 48. The histogram of the differential excitation on skin disease images in the range 0–255 is presented in Fig. 5. WLD finely highlights the strong edges present in the image, which will be useful in the recognition task. Different applications using different versions of WLD are explained in detail in [34].

Experimental Setup and Results

As stated earlier, JUCMATER: Skindb.v1 was used for the experiment that consists of images of three skin diseases Leprosy, Tinea versicolor, and Vitiligo. In addition, the normal skin images were considered to distinguish them from the other three skin disease images. In JUCMATER: Skindb.v1 data set, a total of 876 images of size 144×144 were available. The data set was divided into 4:1 ratio for preparing the training and testing data set. The overall methodology is described in Fig. 1. At first, the region of interest was manually cropped from the camera captured skin lesion image. The only pre-processing employed was the conversion of the color images to the gray scale. The rotation invariant WLD and rotation invariant LBP was applied in this study to get the best micro textural pattern and image gradients from the images in the best competitive environment. Several experiments were done for the skin disease recognition task to achieve the best set of results.

LBP and WLD with rotation invariance, and without rotation invariance was applied on the JUCMATER:Skindb.v1 data set with different P and R values ($[P = 8, R = 1], [P = 16, R = 2], [P = 24, R = 3]$). The multiscale approach was applied to achieve scale invariance and get more discriminate features. The rotation invariant WLD and LBP performed better than normal WLD and LBP individually. In addition, the center of gravity was used to divide the image into sub-regions and then LBP, and WLD features were extracted from each sub-region. The features of LBP and WLD for all the variations were combined to get the benefit of both LBP and WLD. The feature vector size for all such cases is given in Table 1. In addition, the features calculated on the different scales are combined for all such variations. In Table 2, the features at different scales are presented.

While developing the skin disease identification system, the main objective was to identify the feature set that provides the best recognition accuracy. The working methodology and different experimental protocols are described in the following sections. The features acquired under all experiment protocols were used to train a Multi-SVM classifier. The grid search method was applied to find the best regularization parameter(C) and kernel coefficient of rbf kernel(gamma). Here different variations of LBP and WLD were ensembled, and that feature is used in the classification phase. The results using all the experiment protocols are described herein itemized manner.

Table 1 Feature vector size of different versions of LBP and WLD for different (P, R) values

Feature Descriptor	(8,1)	(16,2)	(24,3)
LBP	59	243	555
cogLBP	236	972	2220
WLD	48	48	48
cogWLD	192	192	192
riLBP	10	18	26
cogriLBP	40	72	104
WLDRI	48	48	48
cogWLDRI	192	192	192
WeberLBP	117	291	603
cogWeberLBP	468	1164	2412
riWeberLBP	58	66	74
cogriWeberLBP	232	264	296

Table 2 Feature vector size of different versions of LBP and WLD on combined feature set

Feature Descriptor	Ensembling [(8,1)+(16,2)+(24,3)]
LBP	857
cogLBP	3428
WLD	144
cogWLD	576
riLBP	54
cogriLBP	216
WLDRI	144
cogWLDRI	576
weberLBP	1011
riWeberLBp	198
cogWeberLBP	4044
cogriWeberLBP	792

- **Experiment Protocol 1:** In this experiment protocol, traditional LBP was used in the neighborhood of (8,1), (16,2) and (24,3) to acquire the features at different scales. Accuracy of 74.1379 %, 73.5632% and 73.5632% was achieved using (8,1), (16,2) and (24,3) neighborhoods respectively.
- **Experiment Protocol 2:** The Rotation invariant LBP(riLBP) was used in three different neighborhood (8,1), (16,2) and (24,3) to acquire the features from different scales. Using riLBP 87.931%, 89.0805% and 87.931% accuracy was achieved using (8,1), (16,2) and (24,3) neighborhoods respectively. Using riLBP, significant improvement in the recognition accuracy was achieved. In riLBP, the feature vector size reduced significantly because only the uniform patterns were involved.
- **Experiment Protocol 3:** The WLD and LBP features are ensembled to acquire the strong feature set called WeberLBP and applied in the skin diseases recognition task. Like the previous two experiments three different neighborhood is used. Using WeberLBP 82.1839%, 81.6092% and 86.2069% accuracy was achieved using (8,1), (16,2) and (24,3) neighborhoods respectively. Using the ensemble of LBP and WLD, 8.046%, 8.046% and 12.6437% improvements in the recognition accuracy over the traditional LBP were achieved.
- **Experiment Protocol 4:** The combination of riLBP and WLDRI was used as a strong rotation invariant feature set(riWeberLBP). Accuracy of 87.931%, 89.08085% and 89.0805% accuracy was achieved using (8,1), (16,2) and (24,3) neighborhood. 1.1495% improved accuracy was achieved on (24,3) neighborhood compared to riLBP.
- **Experiment Protocol 5:** The image is divided into four regions using center of gravity, and on each part, the traditional LBP was applied. In this experiment, more detailed information was acquired from the subregions of the image. Accuracy of 79.88%, 75.2874% and 75.2874% was achieved using (8,1), (16,2) and (24,3) neighborhoods respectively using cogLBP. Using cogLBP, 5.7421%, 1.7242% and 1.7242% improved accuracy was achieved over traditional LBP on (8,1), (16,2) and (24,3) neighborhood.
- **Experiment Protocol 6:** Here the rotation invariant LBP was applied to the sub-regions of the image based on the center of gravity. In this experiment, 86.7816%, 90.8046% and 87.3563% accuracy were achieved on (8,1), (16,2) and (24,3) neighborhoods, respectively. 1.724% improved accuracy was achieved compared to traditional LBP on (16,2) neighborhood using cogriLBP.
- **Experiment Protocol 7:** The WLD and LBP were applied to the image's sub regions in this experiment. The center of gravity based WLD and LBP features were combined to form cogWeberLBP. Accuracy of 81.6092%, 81.0345% and 86.78% accuracy was achieved using cogWeberLBP on (8,1), (16,2) and (24,3) neighborhoods respectively.
- **Experiment Protocol 8:** Here, rotation invariant WLD and LBP were applied to the image's sub regions, and the features were combined to form cogriWeberLBP. Using cogriWeberLBP 88.5057%, 91.3793% and 88.5057% accuracy was achieved using (8,1), (16,2) and (24,3) neighborhoods respectively. The cogriWeberLBP achieved the highest accuracy of 91.38% using on (16,2) neighborhood.
- **Experiment Protocol 9:** The features associated with three scales were combined for the LBP, riLBP, WeberLBP, riWeberLBP, cogLBP, cogriLBP, cogWeberLBP, and cogriWeberLBP. The accuracy of multiscale LBP and multiscale riLBP was 81.339% and 81.7664%, respectively. The multiscale WeberLBP and riWeberLBP achieved 83.0484% and 85.4701% accuracy.
- **Experiment Protocol 10:** Some popular deep learning networks like GoogLeNet, MobileNet, ResNet152, DenseNet121, and ResNet101 were applied to the proposed JUCMATER: Skindb.v1 data set to compare the results with the proposed method. Here random flip augmentation was used to increase the size of the data set. ResNet101 achieved 89% accuracy and outperformed the other deep learning models. The results are tabulated in Table 3.

The best accuracy of 91.3793% was achieved using center of gravity based WeberLBP (cogWeberLBP) on (16,2) neighborhood. Results of different experiments using the optimum SVM parameters are tabulated in Table 4. The performance of the proposed approach on the JUCMATER: Skindb.v1 data set was compared with the GLCM, DFT and DCT based methods [2] (Fig. 6). The DCT coefficient based method achieved 73.56% accuracy using Nu value of 0.080 and gamma value of 0.059. The result of the DFT coefficient based method was not good compared to the DCT coefficient based method. The DFT coefficient based approach achieved 70.69% accuracy using Nu value of 0.045 and gamma value of 0.08. The GLCM based approach performed better than the DCT and DFT based techniques and achieved 88.51% accuracy on JUCMATER: Skindb.v1 data set using Nu value of 0.120 and gamma value of 0.070. Whereas the ensemble of center of gravity based rotation invariant WLD and LBP (cogriWeberLBP) achieved 91.38% accuracy, which is significantly better than GLCM, DFT, and DCT based method.

The proposed method results were also compared with some popular deep learning networks such as GoogLeNet, ResNet152, DenseNet121, MobileNet, and ResNet101. A random flip operation was applied on the JUCMATER: Skindb.v1 data set to increase the size of the data set. Using ResNet101, 89% accuracy was achieved, whereas using GoogleNet, ResNet152, MobileNet, and DenseNet121, 73%, 78%,

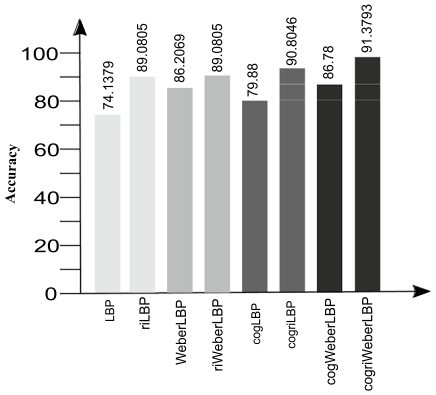

(a) Results of different Proposed Methods

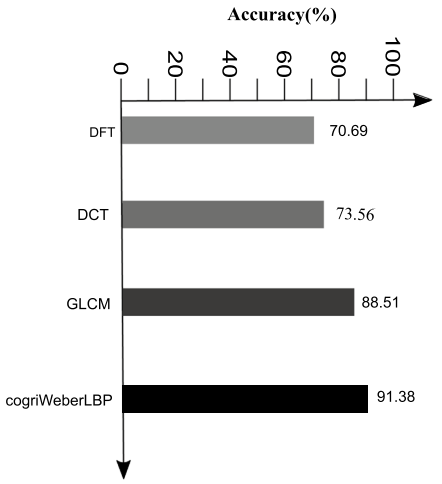

(b) Comparison of Proposed Method with DFT, DCT and GLCM

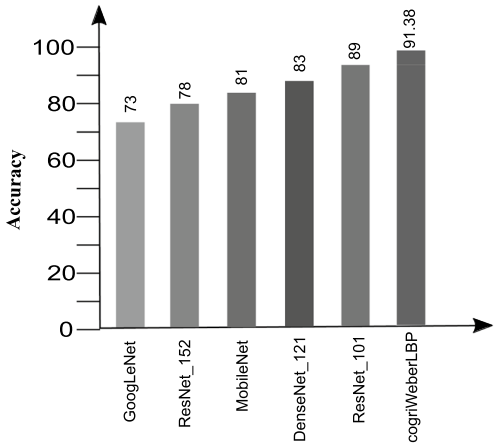

(c) Comparison of Proposed Method with some popular deep learning networks

Fig. 6 Results of proposed methods and comparison with DCT, DFT, GLCM [2] and some popular deep learning networks

81%, and 83% accuracy was achieved accordingly. Despite minimum intra class variation, compared to the previous approaches better accuracy was achieved using the proposed method. But for some of the input images, the skin disease identification system failed to give the correct output. In Fig. 7, some examples of incorrectly detected skin lesion images are depicted. The images of leprosy affected areas with big white patches were incorrectly detected as vitiligo. The normal skin images with red spots were wrongly detected as leprosy because the texture closely matches the initial leprosy symptom. Some misclassifications were also seen in some Tinea versicolor affected skin images and only one vitiligo affected skin image.

Table 3 Comparison of some popular deep learning networks with cogriWeberLBP on the skin diseases data set

Methods	Recognition Accuracy(%)
GoogLeNet	73
ResNet152	78
MobileNet	81
DenseNet121	83
ResNet101	89
cogriWeberLBP	91.3793

Conclusion

Early diagnosing of skin diseases is an important step in the treatment stage. Automatic identification of three similar looking skin diseases—Leprosy, Vitiligo, and Tinea versicolor using the combination of rotation invariant WLD and LBP is proposed in this study. The ensemble of rotation invariant LBP and WLD features from four image regions

(a) Leprosy Detected as Tinea Versicolor

(b) Leprosy Detected as Vitiligo

(c) Normal Detected as Leprosy

(d) Tinea Versicolor detected as Leprosy

(e) Vitiligo detected as Leprosy

Fig. 7 Some examples of incorrectly detected skin lesion image

Table 4 Results of different experiment protocols with best SVM parameters

Methods		(8,1)	(16,2)	(24,3)
LBP	Accuracy	74.1379	73.5632	73.5632
	SVM Parameters	C=512	C=8192	C=512
		Gamma=0.007813	Gamma=0.000122	Gamma=0.000122
riLBP	Accuracy	87.931	89.0805	87.931
	SVM Parameters	C=512	C=8192	C=32768
		Gamma=0.007813	Gamma=0.0078125	Gamma=0.000488
WeberLBP	Accuracy	82.1839	81.6092	86.2069
	SVM Parameters	C=8	C=2	C=8
		Gamma=0.5	Gamma=0.125	Gamma=0.03125
riWeberLBP	Accuracy	87.931	89.0805	89.0805
	SVM Parameters	C=128	C=8	C=8
		Gamma=0.5	Gamma=0.5	Gamma=0.5
cogLBP	Accuracy	79.88	75.2874	75.2874
	SVM Parameters	C=8	C=8	C=32
		Gamma=0.125	Gamma=0.007813	Gamma=0.000488
cogriLBP	Accuracy	86.7816	90.8046	87.3563
	SVM Parameters	C=2	C=8	C=8
		Gamma=2	Gamma=0.5	Gamma=0.5
cogWeberLBP	Accuracy	81.6092	81.0345	86.78
	SVM Parameters	C=8	C=8	C=2048
		Gamma=0.03125	Gamma=0.007813	Gamma=3.05176e−05
cogriWeberLBP	Accuracy	88.5057	91.3793	88.5057
	SVM Parameters	C=8	C=8	C=8
		Gamma=0.125	Gamma=0.125	Gamma=0.125

using center of gravity, cogriWeberLBP gained the best accuracy of 91.38% on JUCMATER: Skindb.v1 data set. The proposed method outperformed the other methods on the same data set. The skin disease recognition accuracy using DFT, DCT, GLCM, and WLD was 70.60%, 73.56%, 88.51%, 89.08% respectively. cogriWeberLBP also outperformed some of the most popular deep neural networks such as MobileNet, ResNet152, GoogLeNet, DenseNet121, and ResNet101. The proposed method achieves a significantly better result than the other texture based approaches and makes the system very robust to recognize diseases without the involvement of specialized doctors. It helps people to automatically check whether they are affected by these skin diseases. This system is especially helpful in rural areas where dermatologists are not available easily. This system can be further improved by gathering more images from the patients and applying different texture descriptors and deep learning techniques.

Data availability The data is under some other research work, so publishing it in some repository is difficult. But, it will be available on genuine request by the researchers. If someone needs it for some academic research only, they can send a request email to researchwork.arnab@gmail.com.

Declarations

Conflict of Interest On behalf of all authors, the corresponding author states that there is no conflict of interest.

References

1. Parekh R, Mittra A. Automated detection of skin diseases using texture features. Int J Eng Sci Technol. 2011;3:4801–8.
2. Das N, Pal A, Mazumder S, et al. An svm based skin disease identification using local binary patterns. In: 2013 Third International Conference on Advances in Computing and Communications, 2013; p. 208–211. https://doi.org/10.1109/ICACC.2013.48.
3. Pal A, Das N, Sarkar S, et al. A new rotation invariant weber local descriptor for recognition of skin diseases. In: Maji P, Ghosh A, Murty MN, et al., editors. Pattern recognition and machine intelligence. Berlin, Heidelberg: Springer; 2013. p. 355–60.
4. Wei LS, Gan Q, Ji T. Skin disease recognition method based on image color and texture features. Comput Math Methods Med. 2018;2018:1–10. https://doi.org/10.1155/2018/8145713.
5. Kabari LG, Bakpo FS. Diagnosing skin diseases using an artificial neural network. In: 2009 2nd International Conference on Adaptive Science Technology (ICAST), 2009; p. 187–191. https://doi.org/10.1109/ICASTECH.2009.5409725.
6. Abdul-Rahman S, Yusoff M, et al. Dermatology diagnosis with feature selection methods and artificial neural network. In: 2012 IEEE-EMBS Conference on Biomedical Engineering and Sciences, 2012; p. 371–376. https://doi.org/10.1109/IECBES.2012.6498195.
7. Yasir R, Rahman MA, Ahmed N. Dermatological disease detection using image processing and artificial neural network. In: 8th International Conference on Electrical and Computer Engineering, 2014; p. 687–690. https://doi.org/10.1109/ICECE.2014.7026918.
8. Codella NCF, Nguyen Q, Pankanti S, et al. Deep learning ensembles for melanoma recognition in dermoscopy images. IBM J Res Dev. 2017;61(4/5):5:1-5:15. https://doi.org/10.1147/JRD.2017.2708299.
9. Thao LT, Quang NH. Automatic skin lesion analysis towards melanoma detection. In: 2017 21st Asia Pacific Symposium on Intelligent and Evolutionary Systems (IES), 2017; p. 106–111. https://doi.org/10.1109/IESYS.2017.8233570.
10. Esteva A, Kuprel B, Novoa R, et al. Dermatologist-level classification of skin cancer with deep neural networks. Nature. 2017. https://doi.org/10.1038/nature21056.
11. Li Y, Shen L. Skin lesion analysis towards melanoma detection using deep learning network. Sensors. 2017. https://doi.org/10.3390/s18020556.
12. Shamsul Arifin M, Golam Kibria M, Firoze A, et al. Dermatological disease diagnosis using color-skin images. In: 2012 International Conference on Machine Learning and Cybernetics, 2012; p. 1675–1680. https://doi.org/10.1109/ICMLC.2012.6359626.
13. Delgado Gomez D, Butakoff C, Ersbøll B, et al. Automatic change detection and quantification of dermatological diseases with an application to psoriasis images. Pattern Recogn Lett. 2007;28(9):1012–8. https://doi.org/10.1016/j.patrec.2006.12.020.
14. Kundu S, Das N, Nasipuri M. Automatic detection of ringworm using local binary pattern (LBP). CoRR abs/1103.0120. 2011, arXiv:1103.0120
15. Übeylı ED, İnan Güler. Automatic detection of erythematosquamous diseases using adaptive neuro-fuzzy inference systems. Comput Biol Med. 2005;35(5):421–33. https://doi.org/10.1016/j.compbiomed.2004.03.003.
16. Schwarz M, Soliman D, Omar M, et al. Optoacoustic dermoscopy of the human skin: tuning excitation energy for optimal detection bandwidth with fast and deep imaging in vivo. IEEE Trans Med Imaging. 2017;36(6):1287–96. https://doi.org/10.1109/TMI.2017.2664142.
17. Chao EK, Meenan CK, Ferris L. Smartphone-based applications for skin monitoring and melanoma detection. Dermatol Clin. 2017. https://doi.org/10.1016/j.det.2017.06.014.
18. Banerjee A, Das N, Nasipuri M, et al. Texture classification using deep neural network based on rotation invariant weber local descriptor. In: Santosh K, Hangarge M, Bevilacqua V, et al., editors. Recent trends in image processing and pattern recognition. Singapore: Springer Singapore; 2017. p. 277–92.
19. Haralick RM, Shanmugam K, Dinstein I. Textural features for image classification. IEEE Trans Syst, Man, Cybern SMC. 1973;3(6):610–21. https://doi.org/10.1109/TSMC.1973.4309314.
20. Conners RW, Harlow CA. Some theoretical considerations concerning texture analysis of radiographic images. In: 1976 IEEE Conference on Decision and Control including the 15th Symposium on Adaptive Processes, 1976; p. 162–167. https://doi.org/10.1109/CDC.1976.267723.
21. Assefa D, Mansinha L, Tiampo KF, et al. Local quaternion Fourier transform and color image texture analysis. Signal Process. 2010;90(6):1825–35. https://doi.org/10.1016/j.sigpro.2009.11.031.
22. Jing XY, Wong HS, Zhang D. Face recognition based on discriminant fractional Fourier feature extraction. Pattern Recogn Lett. 2006;27(13):1465–71. https://doi.org/10.1016/j.patrec.2006.02.020.
23. Ahonen T, Hadid A, Pietikainen M. Face description with local binary patterns: application to face recognition. IEEE Trans Pattern Anal Mach Intell. 2006;28(12):2037–41. https://doi.org/10.1109/TPAMI.2006.244.

24. Shan C, Gong S, McOwan PW. Robust facial expression recognition using local binary patterns. In: IEEE International Conference on Image Processing. 2005; p. II–370. https://doi.org/10.1109/ICIP.2005.1530069.
25. Jun B, Kim T, Kim D. A compact local binary pattern using maximization of mutual information for face analysis. Pattern Recogn. 2011;44(3):532–43. https://doi.org/10.1016/j.patcog.2010.10.008.
26. Liao S, Zhu X, Lei Z, et al. Learning multi-scale block local binary patterns for face recognition. In: Lee SW, Li SZ, editors., et al., Adv Biom. Berlin, Heidelberg: Springer; 2007. p. 828–37.
27. Shan C, Gong S, McOwan PW. Facial expression recognition based on local binary patterns: a comprehensive study. Image Vis Comput. 2009;27(6):803–16. https://doi.org/10.1016/j.imavis.2008.08.005.
28. Xu J, Cha M, Heyman JL, et al. Robust local binary pattern feature sets for periocular biometric identification. In: 2010 Fourth IEEE International Conference on Biometrics: Theory, Applications and Systems (BTAS), 2010; p. 1–8. https://doi.org/10.1109/BTAS.2010.5634504.
29. Lian HC, Lu BL, et al. Multi-view gender classification using local binary patterns and support vector machines. In: Wang J, Yi Z, Zurada JM, et al., editors. Advances in Neural Networks - ISNN 2006. Berlin, Heidelberg: Springer; 2006. p. 202–9.
30. Sun N, Zheng W, Sun C, et al. Gender classification based on boosting local binary pattern. In: Wang J, Yi Z, Zurada JM, et al., editors. Advances in Neural Networks - ISNN 2006. Berlin, Heidelberg: Springer; 2006. p. 194–201.
31. Nanni L, Lumini A. Local binary patterns for a hybrid fingerprint matcher. Pattern Recogn. 2008;41(11):3461–6. https://doi.org/10.1016/j.patcog.2008.05.013.
32. Jin H, Liu Q, Lu H, Tong X. Face detection using improved lbp under bayesian framework. In: Third International Conference on Image and Graphics (ICIG'04), 2004; p. 306–309. https://doi.org/10.1109/ICIG.2004.62.
33. Kundu S, Das N, Nasipuri M. Automatic detection of ringworm using local binary pattern (lbp). Computing Research Repository - CORR 2011.
34. Banerjee A, Das N, Santosh KC. Weber local descriptor for image analysis and recognition: a survey. Vis Comput. 2022;38(1):321–43.